The Internal Seiches in Gullmar Fjord. Part I: Dynamics

LARS ARNEBORG AND BENGT LILJEBLADH

Department of Oceanography, University of Göteborg, Göteborg, Sweden

(Manuscript received 26 July 1999, in final form 20 December 2000)

ABSTRACT

Internal seiche motions with period 1–3 days in Gullmar Fjord are investigated based on mooring data with high vertical and time resolution. The period and structure of the internal seiches are well described by a simple analytical three-layer model taking into account blocking of the basin water at the sill. Energy budgets for forcing and damping of the seiches are estimated. The internal seiches are forced by direct wind stress on the surface and by internal coastal waves of frequency close to the seiches, the latter contribution being a little larger. The *e*-folding timescale for the internal seiche damping is approximately equal to the seiche periods, which means that the seiches are effectively damped, but also that the forcing must be in near resonance in order to maintain the observed seiche motions. In the basin water the seiches manifest themselves with large vertical motions and clear upward phase propagation. The phase propagation is related with a continuous, rather than strictly layered stratification, and can therefore not be described with the three-layer model. It is proposed that the downward energy radiation inherent in the upward phase propagation is caused by removal of energy in the basin water, probably due to dissipation after near-critical reflection from the sloping fjord bottom. The energy flux related to this process is only 2% of the total seiche damping, and therefore not important for the seiche dynamics, which are dominated by the pycnocline movements. In a companion paper, however, it is shown that this energy flux is an important contribution to the increase of potential energy in the basin water due to mixing.

1. Introduction

Internal seiche motions in lakes have been studied intensively because they are often the most energetic motions in the hypolimneon and are therefore important for the vertical mixing (Thorpe 1974; Spiegel and Imberger 1980; Monismith 1985; Wiegand and Chamberlain 1987; and Münnich et al. 1992). In fjords, internal tides, generated by the interaction between the sill and the barotropic tides, are often much more energetic than any other internal motions. Therefore previous work on internal motions and mixing of basin waters in fjords have mainly focused on the internal tides. In Gullmar Fjord the tides are relatively weak, however, and therefore other types of motions can be, and have been, observed. Among these is the barotropic seiche with a period close to 2 h, and the internal seiches with periods varying between 20 and 70 h (Zeilon 1913; Shaffer and Djurfeldt 1983; Djurfeldt 1987; Parsmar and Stigebrandt 1997). In the present paper we study the structure, forcing, and dissipation of the internal seiches in Gullmar Fjord, based on data from two field experiments in the winter and in the late summer of 1997. In a companion paper (Arneborg and Liljebladh 2001) we discuss the contribution from the seiches to basin water mixing in the fjord.

Since the work of Mass and Lam (1995) it is not obvious, theoretically, that internal seiches exist. They showed that it is not always possible to find resonant solutions to the problem of a linearly stratified fluid in a closed container. A more general solution is that of geometric focusing of internal wave energy towards higher wavenumbers concentrated along frequency-dependent closed ray paths. In a linearly stratified fluid resonant basin modes, or seiches, can only be found for certain well-behaved geometries, such as a rectangular basin. Real geometries are not well behaved, but neither are real stratifications linear, and the latter must be the reason why internal seiches are observed. In nature there is often one or more strongly stratified layers, pycnoclines, separating thicker less stratified layers, and the movements of these pycnoclines dominate the fastest-propagating internal waves. In lakes reasonable results have been obtained by comparing observed seiche periods with those predicted by layered models in realistic topographies (Lemmin and Mortimer 1986) or by using normal-mode theory and approximating the lakes with rectangular basins (Wiegand and Chamberlain 1987; Münnich et al. 1992). The only way to explain these results, in view of the results by Maas and Lam (1995),

Corresponding author address: Lars Arneborg, Department of Oceanography, Earth Sciences Centre, University of Göteborg, Box 460, 405 30 Göteborg, Sweden.
E-mail: laar@oce.gu.se

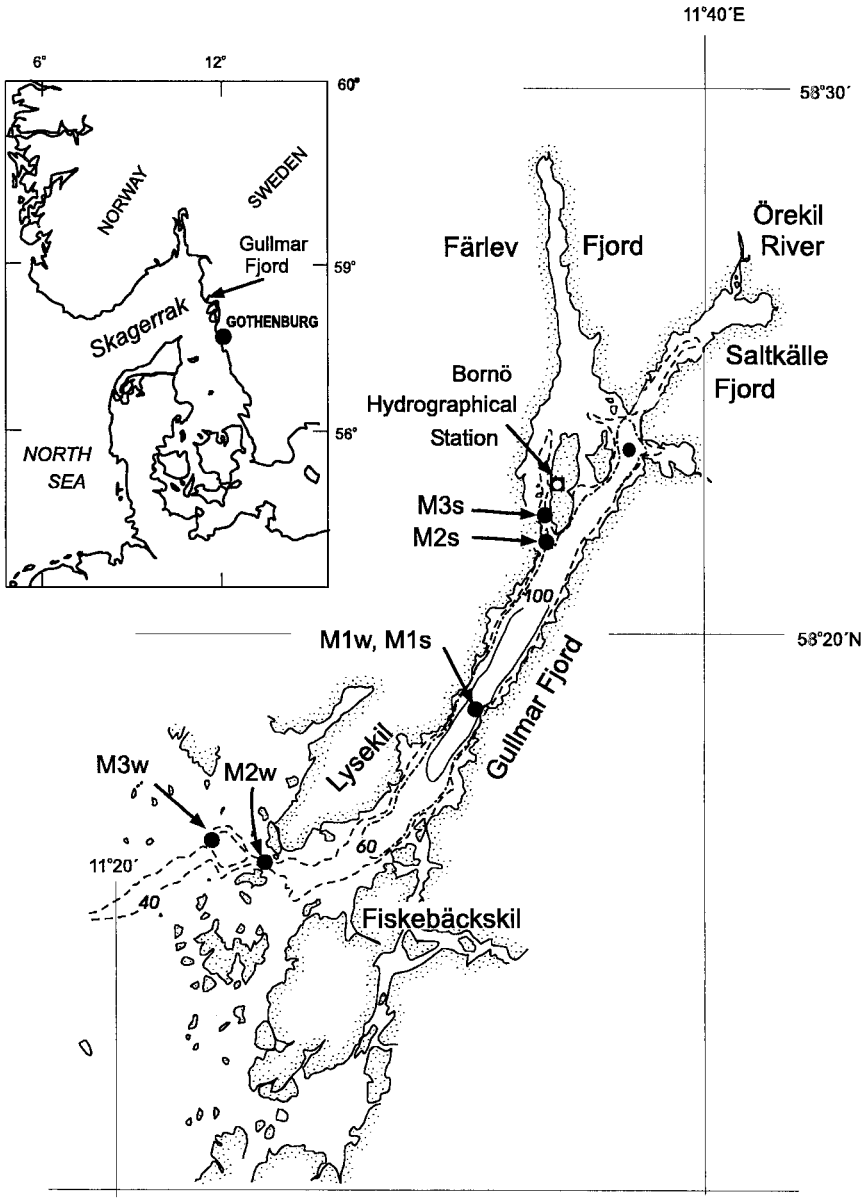

FIG. 1. Sketch of Gullmar Fjord and location of moorings. The moorings M1w, M2w, and M3w were deployed in Jan and Feb 1997, while the moorings M1s, M2s, and M3s were deployed in Aug–Oct 1997.

is that the movements of the pycnocline dominate the seiches. The main purpose of this paper is to investigate large amplitude motions in Gullmar Fjord that have previously been explained as internal seiches (Zeilon 1913; Shaffer and Djurfeldt 1983). Can they be explained by movements of the pycnoclines, How are they forced, and what is the influence of the continuously stratified layers between the pycnoclines?

Gullmar Fjord, Fig. 1, located on the Swedish west coast, is 28 km long and 1–2 km wide with maximum depth 116 m and sill depth 43 m. The inner part of the fjord is branched into the relatively shallow (<40 m) Färlev Fjord, and the somewhat deeper (60 m) Saltkälle Fjord. The freshwater input from Örekil River is weak, only maintaining a fresh surface layer up to 1 m deep in the inner parts of the fjord. The stratification above sill level in the fjord is therefore dominated by the coastal stratification, which varies strongly due to freshwater outflows from the Baltic and wind-driven circulation within the Skagerrak. The water below sill level is stagnant during most of the year, being renewed in late winter most years, though not in the winter of 1997 when one of our field experiments took place. The stratification in the fjord is often characterized by a relatively

strong pycnocline at depth 5–20 m dividing relatively fresh Kattegat water from more saline Skagerrak water. A second, less pronounced pycnocline is often situated just below sill level, separating the Skagerrak water from the denser stagnant basin water. In a winter period and a late summer period of 1997 we deployed three moorings with acoustic Doppler current profilers (ADCPs) and a large number of temperature sensors in and outside the fjord. The data are presented in section 2.

Following the discussion above we expect that that the seiches in Gullmar Fjord are dominated by the movements of the two pycnoclines. But which one is most important, and how do they interact with each other and with the sill? Intuitively one will expect the upper pycnocline to have a resonance similar to a surface seiche with a node at the sill due to the connection with the ocean. But how is the lower pycnocline moving? In section 3 we investigate these questions with a simple three-layer model and compare the results of this model with observations.

Seiches in long lakes are forced by changes in the wind stress, which accelerate the upper layer. For a lake that is narrow relative to the internal Rossby radius the boundary conditions at the lake ends lead to barotropic and baroclinic signals propagating into the lake (Farmer 1978; Monismith 1985). If the dissipation is not too large, these are reflected, eventually leading to internal and external seiches. Resonance occurs if the wind forcing has a periodicity comparable with one of the seiche periods, resulting in large-amplitude motions. The same mechanism works in fjords. In fjords seiches may, however, also be forced by changes in surface elevation and/or stratification outside the fjord. Djurfeldt (1987) did not find any notable seiche motion in Gullmar Fjord during an ice-covered period, which led him to the reasonable conclusion that the internal seiches are mainly forced by local wind. We estimate energy inputs from coastal and from local wind forcing, and reach a different conclusion, as shown in section 4.

A layered model can not be expected to describe all phenomena related with real seiches, which exist in the real continuous stratification. In reality there are upward and downward propagating waves in the continuous stratification related with the pycnocline waves. The length of the wavenumber vector for these waves changes after reflection from a sloping bottom, while the angle relative to horizontal remains constant. This means that the waves leaking out from the pycnocline become unavailable for the pycnocline movements after reflection from the sloping bottom. The importance of these waves depends on the strength of the pycnocline relative to the stratification below (Baines 1982). If the energy flux carried by them is small relative to the energy flux connected with the pycnocline movements, the layered model may be expected to give reasonable results for the overall dynamics. There may, however, still be large internal movements in the weakly stratified layers, which are related with the obliquely propagating waves. In Gullmar Fjord we observe very large movements in the basin water with clear upward phase propagation, indicating that these movements are caused by internal waves propagating downward in the continuously stratified basin water. These observations can obviously not be described by the three-layer theory. In section 5 we discuss the importance of these waves in relation to the overall seiche dynamics and in relation to dissipation of seiche energy in the basin water. The paper is summarized in section 6.

2. The datasets

a. Winter 1997 dataset

In the period 21 January–14 February 1997, three moorings, M1w, M2w, and M3w, were placed in and outside the fjord (see Fig. 1). The deepest mooring, M1w, was equipped with 22 *T, CT,* and *TD* (*T*: temperature, *C*: conductivity, *D*: pressure) sensors and two upward-looking ADCPs, one at the bottom at 107 m and one at 27 m. The second mooring, M2w, was placed in the main entrance to the fjord with two upward-looking ADCPs, one at the bottom at 70 m and one at 15 m. The third mooring, M3w, was placed at 43-m depth outside the fjord with 20 *T, CT,* and *TD* loggers. All ADCPs [RDI Workhorse 300kHz] were configured with 2-m bins and 50 pings/ensemble giving a theoretical standard deviation of $\sim$1 cm s^{-1}, except the one at M1w at 27 m which was configured with 1-m bins and 80 pings/ensemble (standard deviation $\sim$2 cm s^{-1}). The variance may increase substantially at times since backscatter levels vary widely due to vertically migrating plankton. The sampling interval was 10 minutes for all instruments. Generally the conductivity sensors were not accurate enough, so here we only present data from the temperature sensors, which were calibrated with CTD casts taken near the moorings two times during the experiment. In the following we use day numbers as the time coordinate, starting with day 1.0 at 0000 UTC 1 January 1997.

Figure 2 shows temperature and density profiles from CTD casts near moorings M1w at days 21 and 34 and velocities and isotherms at M1w, velocities at M2w, and isotherms at M3w. The general picture is that of relatively warm water at 50–20 m in the beginning of the period overlaid by cold brackish water of Baltic origin. Around day 32 a cold body of water below the pycnocline is advected into the fjord, causing a local temperature minimum at 30–40 m. During the period there is a strong pycnocline at 5–20 m dividing the cold brackish Baltic water from the warmer more saline Skagerrak water. Later in the paper we use the 3.5°C isotherm to represent the location of the pycnocline. Below the pycnocline the water is relatively homogeneous with a small density jump between 60 and 70 m. The low-frequency movements of the coastal pycnocline are closely followed by the pycnocline inside the fjord, with a small

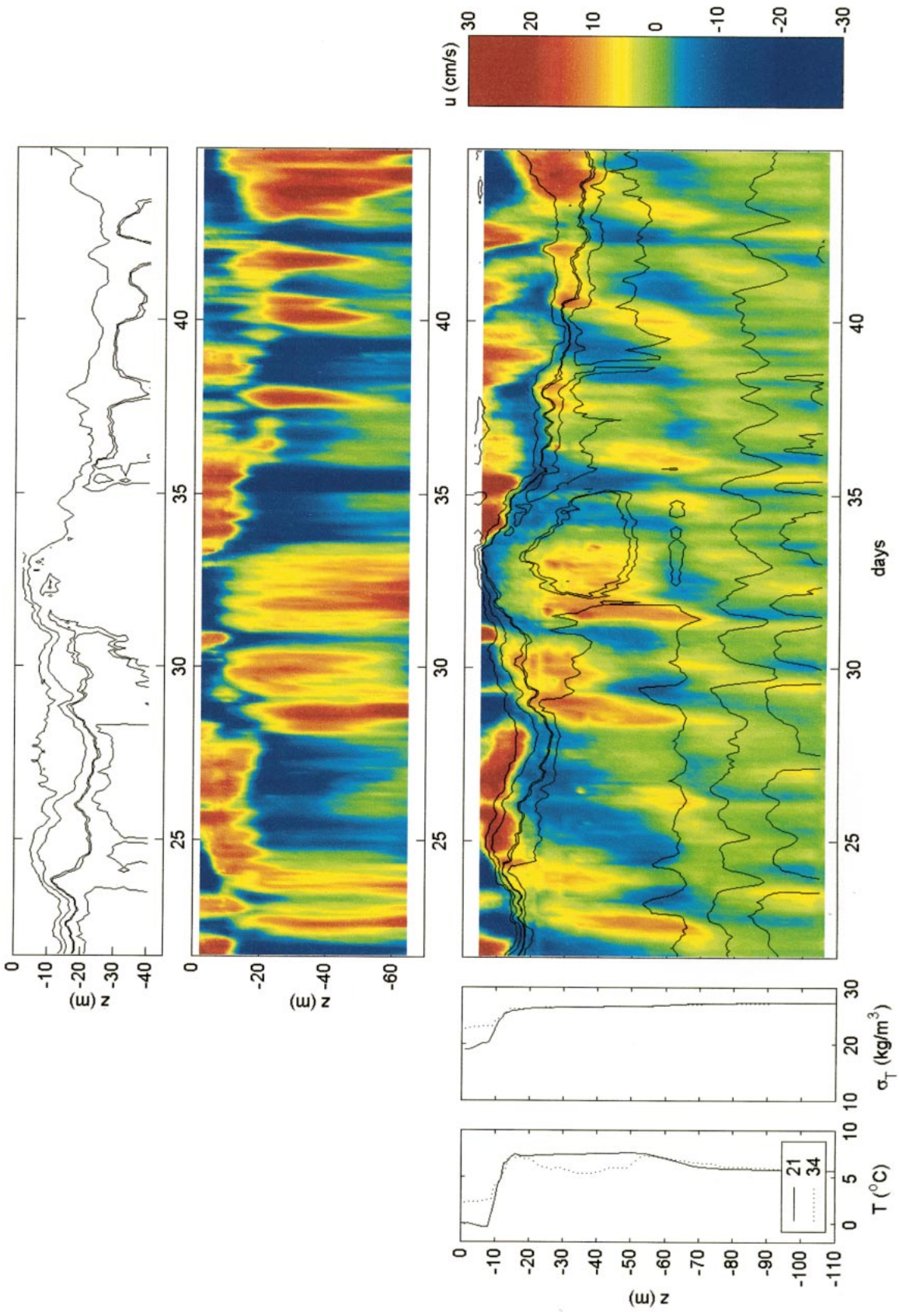

FIG. 2. Isotherms at mooring M3w (upper), velocities at mooring M2w (middle), velocities and isotherms at mooring M1w (lower), and temperature and density profiles from two CTD casts taken near mooring M1w at day 21 and 34. Velocities are projected in the main channel direction with positive values corresponding to inward flow. Isotherms are for 0.0°, 2.0°, 4.0°, 5.8°, 6.0°, and 7.0°C. All time series are 2-h average values.

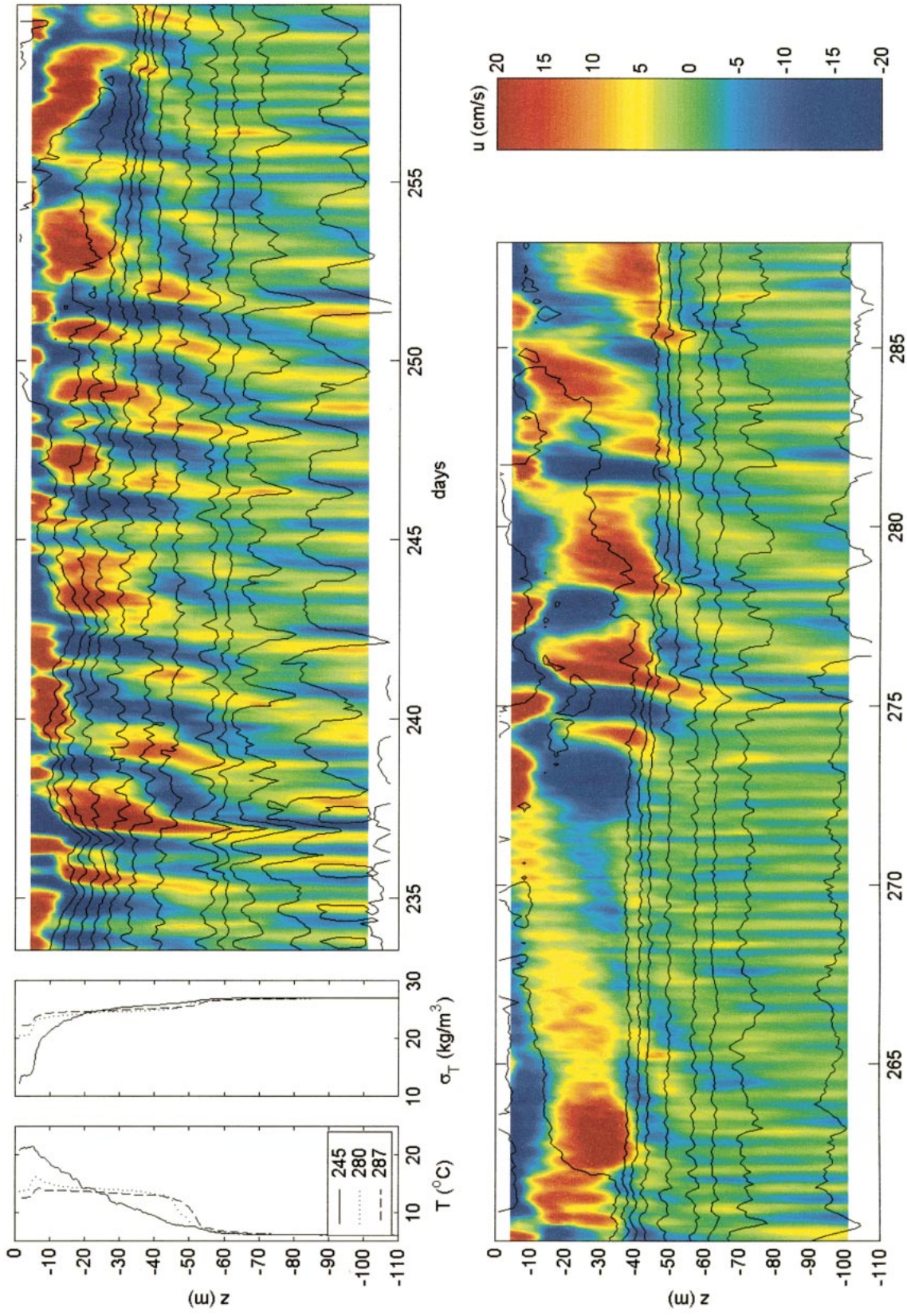

FIG. 3. Velocities and isotherms at mooring M1s and temperature and density profiles from three CTD casts taken near mooring M1s at day 245, 280, and 287. Velocities are projected in the main channel direction with positive values corresponding to inward flow. Isotherms are for 5.995°, 6.05°, 6.2°, 7.8°, 8.0°, 10°, 12°, 14°, 16°, 18°, and 20°C. All time series are 2-h average values.

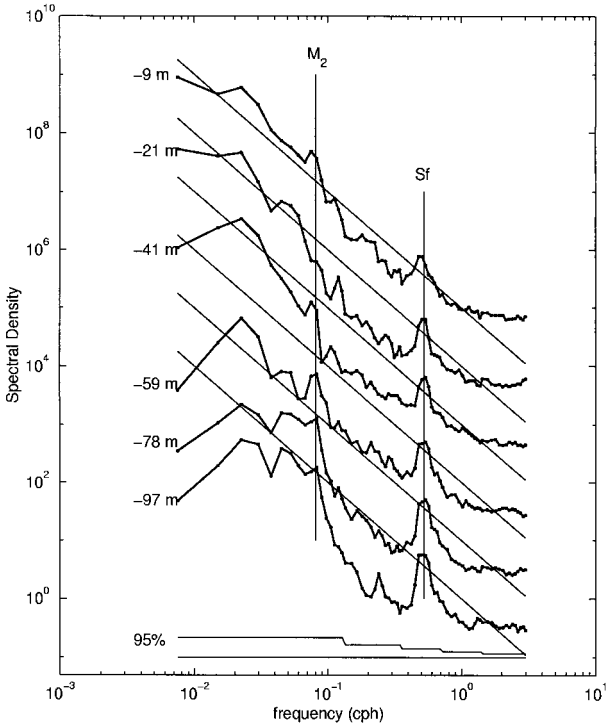

FIG. 4. Spectral estimates of alongfjord velocities at selected depths of M1s. Each spectrum is labeled with its depth. The scale is correct [in $(\text{cm s}^{-1})^2\text{cph}^{-1}$] for the spectrum of the deepest series and is successively offset by one decade for each shallower series. Vertical lines are the M_2 and barotropic seiche (S_f) frequencies. Sloping straight lines are power-minus-two curves. The 95% confidence intervals are shown based on 20 to 320 degrees of freedom in the spectral estimates.

lag (~1/2 day). Below sill level very large amplitude motions of the isotherms are seen. There are a number of strong events with two to three peaks following each other with about 1.5 day interval. These are thought to be connected with internal seiche motions in the fjord, as is discussed later.

b. Late summer 1997 dataset

In the period late August to mid-October 1997 three heavily instrumented moorings, M1s, M2s, and M3s, were deployed inside the fjord (see Fig. 1). The original purpose with the observations was to investigate the reflection of internal waves of tidal and higher frequency on an inner slope of the fjord, which explains the location of M2s and M3s. These results will be presented elsewhere. The inner slope is so steep relative to the characteristics of the internal seiche frequency motions that it acts as a vertical wall for the low-frequency motions with very small horizontal velocities. At 40-m depth the channel opens up into the Färlev Fjord, and above this depth the seiche frequency velocities are generally in phase with the velocities at the same depth at M1s. In this paper we concentrate on mooring M1s.

Mooring M1s was placed at 108-m depth in a narrow section of the main fjord, in order to minimize cross-sectional variations. The mooring was equipped with two upward-looking ADCPs, one at the bottom (RDI, 600 kHz SC-ADCP) and one moored at 55 m (RDI, Workhorse 300 kHz). The bottom ADCP was configured with 4-m bins, 60 pings/ensemble, giving an ensemble standard deviation ~1 cm s^{-1}, and the Workhorse was configured with 2-m bins and similar standard deviation. The 29 *T*, *CT*, *CTD*, and *TD* loggers were distributed with 3–5 m intervals on the mooring. All instruments were sampled with 10-min interval from 21 August to 15 October 1997. The data were calibrated with three CTD casts taken close to the mooring during the period. Again the conductivity sensors were not accurate enough, and therefore we only use and present temperature and velocity data.

Figure 3 shows velocities and isotherms at M1s and temperature and density profiles from CTD casts. The stratification starts out with a strong but not very sharp pycnocline at 10–20 m with a density difference of 8–10 kg m^{-3}. Below the pycnocline the density gradient is continuously decreasing downward, with only a little jump at sill level. Later during the period the density difference over the pycnocline decreases, and the layer between the pycnocline and the sill becomes more homogeneous. A second pycnocline then develops just below sill level. On 7 October the density difference over the upper pycnocline is 3 kg m^{-3}, while over the lower pycnocline it is 1.5 kg m^{-3}. In the CTD profiles the upper pycnocline is located at 5–10 m, which is somewhat misleading since we can see from mooring data that the upper mixed layer oscillates down to 15–20 m.

The velocities above sill level have relatively large amplitudes, up to 20 cm s^{-1} with periods of 1–3 days, except from day 265 to 272 when the situation is relatively calm. In this period one can instead clearly identify the M_2 frequency. Below sill level the velocity oscillations are generally of less amplitude, but very large oscillations are seen in the isotherms in the more homogeneous basin water, similar to what is seen in the winter period.

Spectra of velocities at selected depths of M1s are shown in Fig. 4. The spectra show a clear peak at the barotropic-seiche frequency, S_f (~0.54 cph), less significant peaks at the semidiurnal frequencies (−0.08 cph), and two somewhat diffuse peaks around 0.023 and 0.048 cph. In the plots are also shown power-of-minus-two curves. This is the same frequency dependency as in a Garrett–Munk spectrum for high frequencies, but without the inertial frequency dependency, which we do not expect to be important in a basin narrower than the internal Rossby radius. The uppermost curve follows the power law relatively well, but deeper down the peaks become more distinct. This is an effect of a decrease with depth of energy level between the peaks rather than an increase of the peak energy. For the superinertial frequencies the general energy decrease with depth is

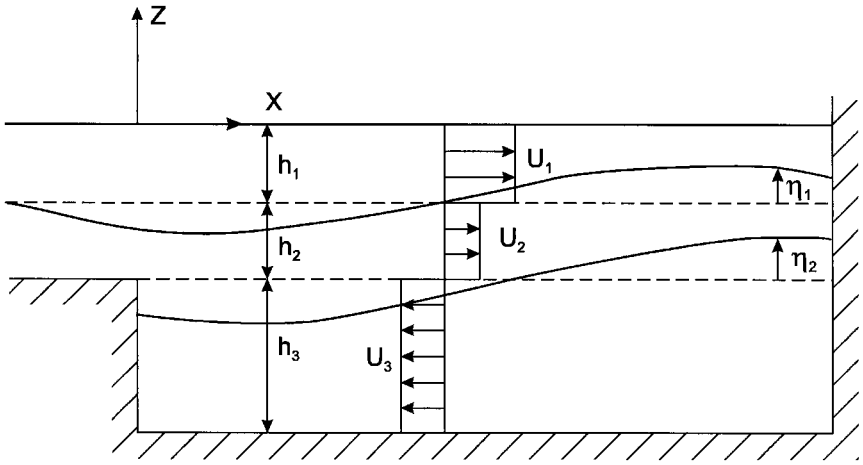

FIG. 5. Definition sketch of model fjord.

in accordance with WKBJ theory in which the energy density is proportional to the buoyancy frequency N.

The two peaks at 0.023 and 0.048 cph are related with the 1–3 day oscillations observed in the time series, which are compared with a three-layer seiche model in the next section. The lowest frequency (0.023 cph) has a significant peak at all depths, but the absolute energy level is largest in the uppermost spectrum at 9 m, somewhat less at 21 and 41 m and much less below the sill. Above the sill, the second frequency (0.048 cph) can only be distinguished from other motions in the spectrum from 21-m depth. Below the sill this frequency has a significant peak at all depths, with the energy level increasing toward the bottom. The energy level at 97 m is comparable with the energy level at 21 m.

3. Seiche dynamics

a. Theory

The vertical density gradient in Gullmar Fjord often has two local maxima, one above sill level and one just below the sill, as seen above. The simplest model that takes into account effects of the sill and both these pycnoclines is a linear-theory, one-dimensional, three-layer model with a box-shaped fjord, open toward the coast in the two upper layers (Fig. 5). We are interested in frequencies lower than the inertial frequency and a fjord much narrower than the internal Rossby radius, which means that we can neglect cross-fjord variations. The linearized equations for free motions of three superposed shallow layers with uniform depths h_i, $i = 1, 2, 3$, can, after use of the rigid-lid and Boussinesq approximations and after transformation into normal-mode form (Gill 1982), be written as

$$\eta_{1tt} - c_n^2 \eta_{1xx} = 0, \tag{1}$$

in terms of the upper-interface elevation η_1. The lower interface is related to the upper interface through

$$\eta_2 = \mu_n \eta_1, \tag{2}$$

where the eigenvalue, μ_n, satisfies the characteristic equation

$$\mu_n^2 + \left(\frac{g_1'(h_2 + h_3)}{g_2' h_3} - \frac{h_1 + h_2}{h_1} \right) \mu_n - \frac{g_1'}{g_2'} = 0, \tag{3}$$

and the phase velocity c_n can be found from

$$c_n^2 = \frac{g_1' h_1 h_2}{h_2 + (1 - \mu_n) h_1}, \tag{4}$$

where g_1' and g_2' are the reduced gravitational accelerations at the two interfaces. The two solutions of (3) correspond to the two baroclinic modes. The velocities in each layer are related to the interface elevations through

$$u_{1x} = \frac{1}{h_1} \eta_{1t}, \tag{5}$$

$$u_{2x} = \frac{1}{h_2} (\eta_{2t} - \eta_{1t}), \tag{6}$$

$$u_{3x} = -\frac{1}{h_2} \eta_{2t}. \tag{7}$$

At the inner wall, $x = L$, (1) is subject to the boundary condition $u_i = 0$, $i = 1, 2, 3$. Using the horizontal momentum equations (these are not explicitly stated here) this can also be written as

$$\eta_{1x}(L, t) = 0. \tag{8}$$

Inserting the time dependency $\exp(-j\omega t)$ into (1), the solutions that satisfy the boundary condition (8) can be written as

$$\eta_1(x, t) = \sum_{n=1}^{2} A_n \cos\left[\frac{\omega}{c_n} (x - L) \right] e^{-j\omega t}, \tag{9}$$

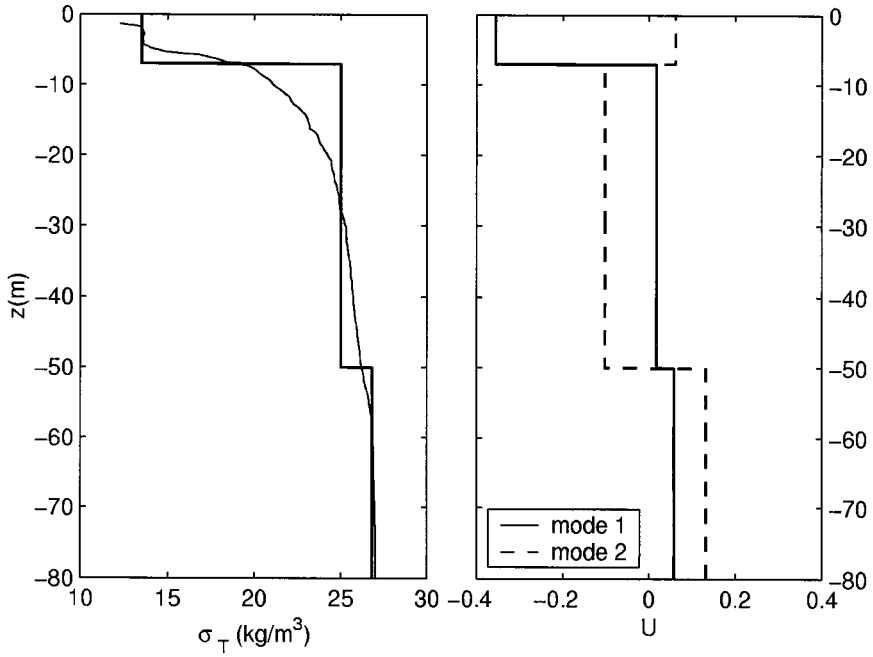

FIG. 6. Model and real stratification (a), and velocity modes corresponding to model stratification (b).

where A_n is the amplitude of upper-layer interface elevation at the inner wall, caused by the nth mode. At the mouth, $x = 0$, the boundary conditions are more complicated. Below sill level the horizontal velocity is zero. Using (1), (2), (7), and (9) this can be written as

$$\sum_{n=1}^{2} A_n c_n \mu_n \sin(\omega L/c_n) = 0. \tag{10}$$

Above the sill there must be a radiation condition in order to determine a relation between the upper-interface elevation and the velocities in the two upper layers. The radiation boundary condition depends on the topography outside the mouth. A reasonable approximation to the coast outside the fjord is that of a wall at $x = 0$ bounding a semi-infinite ocean of constant depth $h_1 + h_2$, that is, with the same depth as the sill. At subinertial frequencies coastal Kelvin waves are the only possible motions that can radiate energy away from the fjord mouth. In order to determine an appropriate radiation condition we use a black-box approach, where details of the flow close to the mouth are not known but where a connection is found between the flow in the fjord and the flow in the coastal Kelvin wave. This connection is found by assuming continuity of baroclinic mass fluxes and baroclinic energy fluxes between the fjord mouth, at $x = 0$, and a cross-coast section just downstream (in the sense of Kelvin wave propagation) from the fjord, say at $y = 2W$, where W is the fjord width. In the appendix it is shown that this condition combined with (10) can be written as

$$\frac{1}{2}\frac{W}{a_i} = -j\frac{\mu_2\mu_1}{\mu_2 - \mu_1}\left(\frac{c_i}{\mu_1 c_1}\cot\left(\frac{\omega L}{c_1}\right) - \frac{c_i}{\mu_2 c_2}\cot\left(\frac{\omega L}{c_2}\right)\right), \tag{11}$$

where c_i and a_i are the baroclinic phase velocity and Rossby radius outside the fjord, defined by and related through

$$fa_i = c_i \equiv \left(\frac{g_1' h_1 h_2}{h_1 + h_2}\right)^{1/2}, \tag{12}$$

where f is the Coriolis parameter. The solutions to (11) are complex with the real part being the angular frequency of oscillation and the imaginary part being the inverse damping timescale. The damping is caused by loss of energy to the coastal wave. If the width of the fjord is small relative to the internal Rossby radius, the lowest-order approximation to (11) is

$$0 = \frac{1}{\mu_1 c_1}\cot\left(\frac{\omega L}{c_1}\right) - \frac{1}{\mu_2 c_2}\cot\left(\frac{\omega L}{c_2}\right). \tag{13}$$

This relation can also be obtained by specifying zero velocity in the lower layer and zero elevation of the upper interface at the mouth. After having solved for the eigenfrequencies from (11) or (13), the relation between the vertical mode amplitudes A_n can be found from (10), the lower-layer amplitudes from (2), and the horizontal velocities from (5)–(7). It is important to note that both vertical mode amplitudes must be different

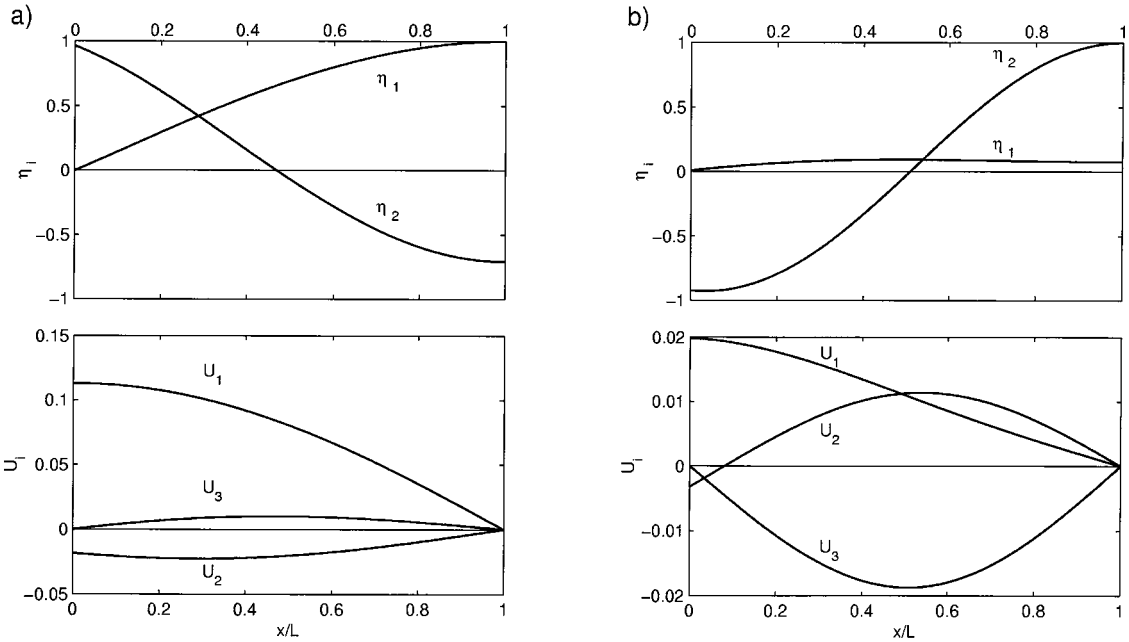

FIG. 7. Interface elevation and horizontal velocity amplitudes as a function of the x coordinate for first seiche at frequency 0.029 cph (a) and second seiche at frequency 0.042 cph (b). The shown seiching modes are normalized with respect to the maximum interface elevation.

from zero to fulfill (10). This is because one single mode cannot fulfill both the conditions of zero velocity in the lower layer and zero upper-interface elevation.

b. Model results

We have chosen to investigate a three-layer stratification representing the stratification at the beginning of the summer–fall experiment in Gullmar Fjord, described above. The real stratification and the model stratification are shown in Fig. 6 together with the two velocity modes. The relevant model parameters are given in Table 1.

The width of Gullmar Fjord is 1–2 km, so the maximum value of W/a_i is 0.3, which means that a reasonable approximation to the eigenfrequencies can be found by solving (13). The equation has an infinite number of solutions, of which the two lowest-frequency solutions are described here.

For a fjord with the shown stratification and a length 25 km the frequency of the first (lowest frequency) seiche, found from (13), is 0.029 cph (34 h), while the frequency of the second seiche is 0.042 cph (24 h). The velocity- and interface-elevation shapes of these seiches are shown in Fig. 7. The first seiche is a quarter-wave on the upper pycnocline with the main horizontal motions taking place in the two upper layers and the lower layer being blocked by the presence of the sill. The second resonance is a half-wave on the lower pycnocline with almost no vertical motion of the upper pycnocline. The horizontal motions in the upper layer, though, are still relatively large. The above results are sensitive to the relative strength and location of the two pycnoclines, mainly with regard to the seiche periods. For example, a lowering of the upper pycnocline and a weakening of the lower pycnocline will make the internal waves on the lower pycnocline slower, and the ones on the upper pycnocline faster, so that the half-wave resonance on the lower pycnocline may attain a longer period than the quarter-wave resonance on the upper pycnocline.

TABLE 1. Parameters used in the model.

Input parameters		Derived parameters	
g_1' (m s^{-2})	0.113	μ_1	0.702
g_2' (m s^{-2})	0.020	μ_2	−9.11
h_1 (m)	7	c_1 (m s^{-1})	0.868
h_2 (m)	43	c_2 (m s^{-1})	0.546
h_3 (m)	30	c_i (m s^{-1})	0.824
L (m)	25 000	a_i (m)	6700

c. Comparison with observations

The two somewhat diffuse peaks at 0.023 and 0.048 cph, observed in the spectra (Fig. 4), correspond reasonably with the values 0.029 and 0.042 cph predicted from the three-layer seiche model. In order to test whether the vertical structure also fits with those predicted by the model, we perform empirical orthogonal function analysis in the frequency domain (FEOF) as described in Djurfeldt (1987).

The FEOF analysis is performed on the spectra of 13 velocity time series at M1s separated from each other by approximately 8 m. The analysis is performed on the

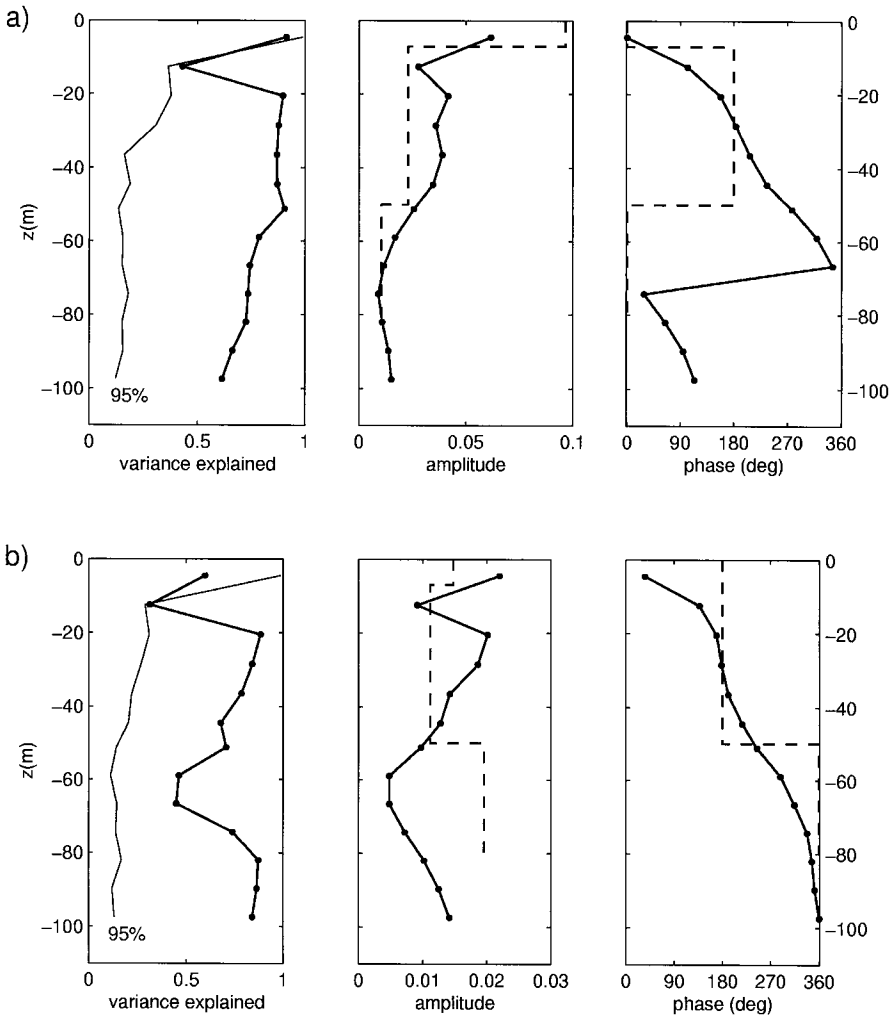

FIG. 8. FEOF velocity modes for the frequency bands (a) 0.018–0.034 cph, and (b) 0.034–0.051 cph, showing the fraction of the total variance within each frequency band, explained by the first FEOF mode, and the amplitudes and phases of the modes. In the variance plots the 95% significance levels are also shown. These are found from Monte Carlo simulation with 100 synthetic datasets with the same band-averaged variances as the real data. Dashed lines show model velocities and phases at $x/L = 0.4$ for the first (a) and second (b) internal seiche frequency.

whole 55-day late summer series. Figure 8 shows the most variance-explaining mode from the bands 0.018–0.034 cph and 0.034–0.051 cph, which are obtained by averaging over 22 frequency bins. The most variance-explaining mode in each of the two frequency bands explains 82% and 71% of the variance within their frequency bands. Confidence estimates are obtained with the Monte Carlo method presented in Djurfeldt (1987). The 95% confidence limits for the first modes are 47% and 44% in the two frequency bands, which shows that the modes are statistically significant. In Fig. 8 we also show the 95% confidence limits for each point in the modes. The very large value for the confidence limit at the surface is due to the large variance in this time series, which dominates the analysis. This problem can be avoided by normalizing the time series. We have, however, tested the analysis with different normalizations, and found that the results are very insensitive to these. Included in Fig. 8 are the velocity structures as predicted by the three-layer model at $x/L = 0.4$, which corresponds to the location of M1s. The amplitude of the velocity structure is scaled to fit approximately with the observed FEOF structure amplitudes.

The frequency band 0.018–0.034 cph is characterized by large velocities at the surface and somewhat smaller velocities between 20 and 40 m depth, decreasing down to 70 m, with a little increase toward the bottom. The phase changes with almost 180° from the surface to depth 20 m, where it is relatively constant down to 40 m, followed by an almost linear phase change toward

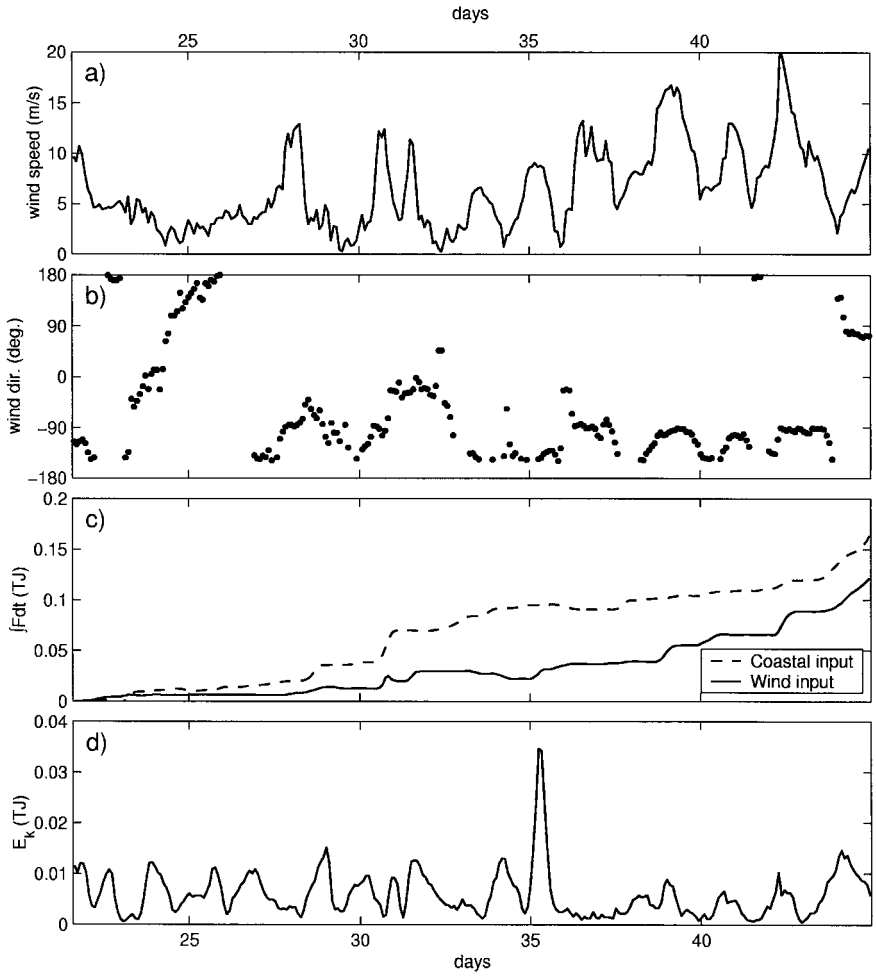

FIG. 9. Time series from the winter period, showing 2-h-averaged wind speed (a) and wind direction (b) from Kristineberg, time-integrated energy input to the seiches by the wind and through the mouth (c), and fjord integrated kinetic energy.

the bottom with a phase difference of 180° between 30 and 70 m. The variance at 15-m depth is not very large. This is probably due to the movement of the pycnocline, which causes this depth to be located sometimes above and sometimes below the pycnocline. Comparing with the velocity structure predicted by the three-layer model we see that the three-layer model also has maximum amplitude in the upper layer, smaller amplitude in the intermediate layer, and smallest amplitude in the lower layer, although the relative differences are not predicted very well. The continuous phase changes in the FEOF results can naturally not be described in the three-layer model, as discussed in section 5, but the average phases within each layer are well predicted by the model, and the FEOF results are seen to have largest phase gradients at the location of the 180° phase shifts in the model.

In the frequency band 0.034–0.051 cph the most variance-explaining mode has statistically significant movements only below depth 20 m, which means that we cannot conclude anything about the upper-layer movements. The movements below 20 m are characterized by relatively large velocities at 20 m, decreasing toward 60 m, and increasing again toward the bottom. The magnitude of the bottom velocities is about 70% of the velocities at 20 m. The phase is relatively constant between 20 and 40 m, shifting about 180° down to 70 m and, again, being relatively constant toward the bottom. Model results at $x/L = 0.4$ show largest velocities in the lowest layer, 180° out of phase with the velocities in the two upper layers. In the model the intermediate-layer velocity is only about half as large as the velocity in the lower layer. Although the quantitative properties are not exactly equal, the relatively sharp phase shift at sill level in the observations shows that the lower-pycnocline movements are important for this frequency band. This indicates that the spectral peak at 0.048 cph is caused by a half-wave resonance on the lower pycnocline, as the model predicts.

It is seen that the spectral peaks at 0.023 and 0.048 cph are relatively well predicted by a three-layer seiche

model with respect to both the frequencies and the vertical variations of the horizontal velocities. One cannot expect perfect agreement when considering the simplicity of the model with respect to both topography and stratification. For example, we have not taken into account the branching of the fjord or that the fjord is shorter at the depth of the lowest pycnocline than at the depth of the upper pycnocline. Neither have we taken into account that the stratification changes during the measurement period. Anyway, based on the reasonable agreement between the model and the observations, we conclude that (i) the spectral peak around 0.023 cph is dominated by the movements of the upper pycnocline with a node at the sill and the lower-layer motions being blocked by the sill, (ii) the movements of the lower pycnocline dominate the spectral peak around 0.048 cph with a node in the middle of the fjord, and (iii) a basin mode (seiche) in a fjord cannot be explained as a single vertical mode with a certain horizontal structure. Each basin mode is a superposition of all (two in the three-layer case) vertical modes, each with their horizontal structure, and these are coupled by the topography at the sill.

4. Forcing and damping

The presence and duration of a seiche in a fjord is dependent on the forcing and damping mechanisms. If the damping is too large, the seiche will never be able to show up, and, if the damping is very small, the seiche can execute many oscillations. In Gullmar Fjord the internal seiches are such prominent features that one wonders whether the damping is very small or whether the seiches are close to being in resonance with the forcing so that these are kept going in spite of strong damping. If the latter is the case, the seiches can be important contributors to mixing in the fjord.

a. Theory

The damping can be determined with different methods. One method is to estimate the damping from the width of the spectral peak. In our case the widths of the spectral peaks are, however, dominated by variations of the resonance frequencies due to variations in the stratification rather than by the damping. Another method is to find a time where the forcing is zero and then determine the damping from the decay of the seiches. A third method is to set up an energy budget for the sources and sinks of mechanical energy in the internal seiches. The last method is used in this paper since we have a dataset that gives us the possibility to estimate the forcing terms over many seiche events.

Assuming that we can separate the motions connected with the seiches from the lower-frequency motions, the equations for the perturbation kinetic and potential energy, E_k and E_p, integrated over the fjord, become

$$\frac{\partial E_k}{\partial t} + \frac{\partial E_p}{\partial t} = F_m + F_w - D, \tag{14}$$

where F_m is net energy input through the mouth, F_W is energy input by the wind, and D is energy loss due to damping of the seiche. The damping term D contains energy losses to side and bottom friction, net energy loss to other frequencies, and direct production of turbulent kinetic energy. It is appropriate to note that the energy loss due to outward radiation is contained within the term F_m, which can therefore be both positive and negative. The energy input by wind can also be negative if, for example, the forcing through the mouth sets up a seiche out of phase with the wind forcing. However, the damping term, D, may always be expected to be positive.

By assuming two-layer theory, the energy input through the mouth can be written as (for further details see appendix)

$$F_m = \Delta\rho g \overline{Q_2 \eta}, \tag{15}$$

where Q_2 is the baroclinic volume flux in the lower layer, $\Delta\rho$ the density difference between the layers, and η the elevation of the interface. Assuming that the shear stress at the bottom of the surface mixed layer is negligible compared with the wind shear stress, the part of the energy input by the wind that is used to increase the perturbation mechanical energy can be written as

$$F_w = \int_{A_s} \overline{\tau_w u_{\mathrm{ML}}}\, dA, \tag{16}$$

where τ_w is the shear stress from the wind on the surface, u_{ML} is the mean velocity in the surface mixed layer, and A_s is the surface area of the fjord.

After writing the damping D as $D = CE_k$ we can estimate the damping coefficient C by integrating (14) over a long enough time interval (many seiche periods) that the left-hand side becomes negligible relative to the terms on the right-hand side. The damping coefficient can then be found as

$$C = \frac{\int_{t_1}^{t_2} (F_m + F_w)\, dt}{\int_{t_1}^{t_2} E_k\, dt}. \tag{17}$$

In analogy with a single-degree-of-freedom system the transition between oscillatory and overdamped response (critical damping) is found when $C = C_c = 4\omega$, where ω is the angular frequency of the undamped seiche.

b. Results

We use the winter data to estimate the energy budget since we have data outside the fjord and in the fjord mouth in this period. The perturbation energies are here

defined as those connected to motions with frequencies above 0.01 cph and below semidiurnal frequencies, and we obtain these by bandpass filtering the time series in the band 0.01–0.07 cph before determining the energies and energy fluxes. The period from day 21 to day 45 is characterized by a strong pycnocline, and it is therefore possible to use the two-layer expression in (15) to estimate the baroclinic energy flux through the mouth. During this period the pycnocline at M3w is well represented by the location of the 3.5°C isotherm. The interface elevation η is therefore found by determining the location of the 3.5°C isotherm from linear interpolation and then bandpass filtering the time series. The volume flux Q_2 is found by integrating the velocities at M2w, multiplied with the width of the channel, from the bottom to the interface, and then bandpass filtering the signal. The density difference over the interface is found by averaging available density data above and below the interface at M3w. The time-integrated energy input is shown in Fig. 9c. The average energy input is $F_m = 81$ kW: The energy flux estimated this way is the net input of baroclinic energy, which is the difference between the inward and outward radiating energy. It is interesting that the cumulated net energy input is almost monotonically increasing; that is, the inward energy radiation is always larger than the outward. This suggests that damping due to friction and energy dissipation inside the fjord (represented by the term D) is larger than damping due to outward radiation. If outward radiation was important for the seiche damping, one would expect periods with strong forcing (steep positive slope in Fig. 9c) to be followed by periods with negative forcing (negative slope in Fig. 9c), and this is not the case.

The wind input is estimated using 2-h-averaged wind data from Kristineberg (Fig. 1; see Figs 9a and 9b). The alongfjord shear stress is calculated as

$$\tau_w = C_d \rho_a w_f w, \tag{18}$$

where $C_d = 0.0011$ is a drag coefficient, $\rho_a = 1.2$ kg m^{-3} is air density, w_f is wind velocity projected in the main fjord direction, and w is wind speed. When calculating the energy input from (16), using the wind at Kristineberg and the velocities at M1w, it is necessary to assume something about the spatial distribution of the wind and the surface velocity over the fjord area. We assume that the wind at Kristineberg is representative of the wind field over the main part of the fjord. Concerning the velocities one may expect that these are increasing toward the mouth due to the quarter-wave structure of the upper-pycnocline movements (see section 3), and, in addition, there must be a local maximum at M1w because the fjord is relatively narrow there. To account for these effects we assume that the seiche is a standing wave with a node at the sill and an antinode at the inner end of the fjord. A standing wave is a superposition of two waves of equal amplitude, each propagating in opposite directions. If we assume constant depth and similarity between the fjord cross-sections, the horizontal velocity at a given depth can be written as

$$\begin{aligned} u(x, t) &= U(x)[\sin(kx - \omega t) + \sin(-kx - \omega t)] \\ &= 2U(x)\cos(kx)\sin(-\omega t), \qquad k = \frac{\pi}{2L}, \end{aligned} \tag{19}$$

where $U(x)$ is the horizontal velocity amplitude of each of the two waves at the considered depth. The energy flux in each of the two waves is constant along the length of the fjord, which leads to the result that $U(x)$ is related to the width of the fjord, W, through

$$U(x)^2 W(x) = \text{const.} \tag{20}$$

From (19) and (20) it can be shown that the horizontally averaged velocity amplitude, $\langle u \rangle$, at a given depth can be written in terms of the velocity amplitude, u_{M1w}, at the same depth at M1w, as

$$\langle u \rangle = u_{\mathrm{M1w}} \frac{W_{\mathrm{M1w}}^{1/2}}{A\cos(kx_{\mathrm{M1w}})} \int_0^L \cos(kx) W^{1/2}\, dx, \tag{21}$$

where A is the horizontal area of the fjord at the given depth, while W and W_{M1w} are the z-dependent fjord widths at x and x_{M1w}, respectively.

The widths at the surface are given for 1000-m segments in Zeilon (1913). Inserting these in the discrete version of (21), we get that the relation between the horizontally averaged surface-layer velocity, $\langle u \rangle$ and the surface-layer velocity at M1w, u_{M1w}, is $\langle u \rangle = 0.51 u_{\mathrm{M1w}}$. The surface area of the fjord is $A_s = 51 \times 10^6$ m^2. The surface-layer velocity at M1w is found as the average velocity above the 3.5°C isotherm. The energy input by wind is found by multiplying the estimated average surface-layer velocity with the wind stress found from (18) and the surface area. The time-integrated wind energy input calculated this way is shown in Fig. 9c. The average energy input by local wind is $F_w = 60$ kW, that is, slightly smaller than the energy input through the mouth. It is also seen that the input by local wind is largest in the last period when the wind direction is mainly southwesterly (in the fjord direction) during strong wind events, while the input through the mouth is largest in the beginning when the wind direction is west to north during strong wind events.

When calculating the kinetic energy we use the same basic assumption as above regarding the horizontal velocity distribution. The total kinetic energy in the fjord can then be described in terms of the velocities at M1w by

$$\begin{aligned} E_k &= \frac{1}{2}\rho_0 \int_{-H}^{0} \int_0^L u^2 W\, dx\, dz \\ &= \frac{1}{4}\rho_0 \int_{-H}^{0} \frac{u_{\mathrm{M1w}}^2}{\cos(kx_{\mathrm{M1w}})^2} \frac{W_{\mathrm{M1w}}}{\langle W \rangle} A\, dz, \end{aligned} \tag{22}$$

where $\langle W \rangle$ is the horizontal averaged width of the fjord at level z. As a good approximation we can set $W_{\mathrm{M1w}}/$

($\langle W\rangle \cos(k\, x_{\mathrm{M1w}})$) constant with depth. Using the values for W_{M1w} and $\langle W\rangle$ at the surface gives

$$E_k = \frac{1}{2}\rho_0 \int_{-H}^{0} 0.33 u_{\mathrm{M1w}}^2 A \, dz. \tag{23}$$

In Fig. 9d we show an estimate of the kinetic energy in the fjord, calculated from (23). The average kinetic energy over the period is, $E_k = 5.9$ GJ.

It is now possible to find the damping coefficient C from (17). The result is $C = 2.4 \times 10^{-5}\ \mathrm{s}^{-1}$. Comparing with the angular frequency ω of the 0.023-cph seiche, we obtain $C = 0.60\omega$. The e-folding scale, T_e, is related to the damping coefficient through $T_e = 4/C$. With the results above we get that the ratio between the e-folding scale and the period of the seiche is $T_e/T = 1.1$; that is, the seiche is damped after approximately one wave period. The ratio between the actual damping and the critical damping C_c is, $C/C_c = 0.15$; that is, although the damping is strong, the seiche is still underdamped. It must be remembered that the damping estimated above does not include damping from outward radiation and active damping by the wind. The actual damping of the seiche may therefore be even larger. Based on the curves in Fig. 9c and the comments above, we expect, however, that these effects are of minor importance relative to the internal damping estimated here.

That the seiches are observed often and with large amplitudes, even though the damping is strong, must be due to near resonance of the forcing. This is not unreasonable since the low atmosphere pressure systems coming in from the west, which in the end are the cause for the seiches either by forcing inside or outside the fjord, often have timescales of 1–3 days.

5. Basin water motions

The results in section 3 show that the main dynamics of the internal seiches are well predicted by a simple three-layer theory. This probably means that the relatively sharp pycnoclines are important for the generation, propagation, and reflection of the internal waves that constitute the internal seiches. There are, nevertheless, a number of interesting features in the measurements not accounted for in the model, which are related to the continuous stratification between the pycnoclines and in the basin water and to the real, rather than box-formed, topography. These are the continuous phase change observed in the lowest-frequency seiche as mentioned in section 3 and the large amplitude of the vertical displacements in the basin water. The FEOF analysis in section 3 shows that the phase at a given time is decreasing upward. This corresponds to a positive upward phase velocity. Internal waves with upward phase propagation are known to have downward energy propagation. A possible explanation for the upward phase propagation therefore is that we see an internal wave with downward energy propagation, or at least a combination of waves with a dominating downward radiation.

One way to investigate the properties of these motions is to look at the relation between the vertical displacements and the horizontal velocity. Figure 10 shows the coherence-squared, transfer function and phase angle between vertical displacement and horizontal velocity at 82-m depth. For a single obliquely propagating internal wave the relation between the amplitude of horizontal velocities, u_0 and the amplitude of vertical displacements, VD_0, can be found to be

$$\frac{u_0}{VD_0} = \sqrt{N^2 - \omega^2} \approx N, \tag{24}$$

where N is the buoyancy frequency.

In Fig. 10 it is seen that the coherence is very large around the internal seiche frequencies, and at the lowest seiche frequency (0.023 cph) the ratio between the velocity amplitude and the vertical displacement amplitude is 0.005 s^{-1}. The buoyancy frequency at 80 m is $N = 0.006\ \mathrm{s}^{-1}$, which shows that (24) is close to being fulfilled. The vertical displacement lags the horizontal velocity with about $-86°$ at this frequency. In a single obliquely propagating wave the vertical displacement lags the horizontal velocity with $\pm 90°$, depending on the direction of the wave. For a wave with downward energy propagation the sign is negative (positive) for

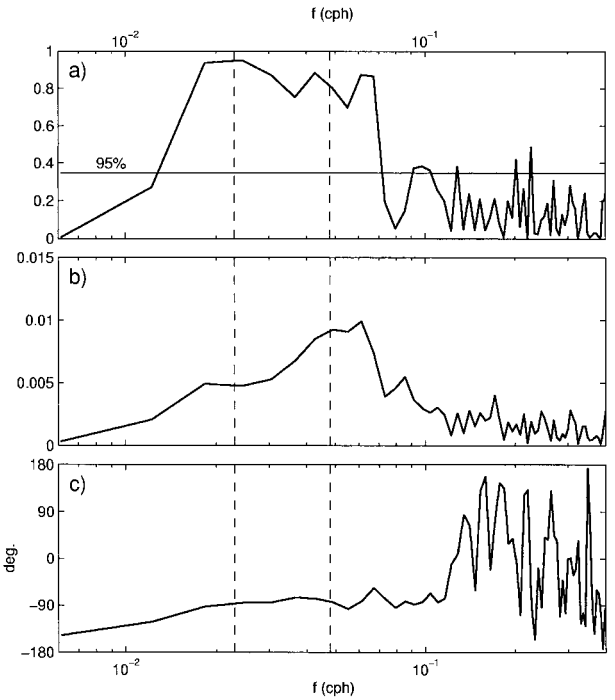

FIG. 10. Coherence-squared (a) and amplitude (b) and phase (c) of the transfer function from the vertical displacement to the horizontal velocity at depth 82 m, based on whole time series at M1s. The horizontal dashed line is the 95% confidence limit for coherence, corresponding to 16 degrees of freedom, while the vertical dashed lines are the frequencies of the first and second internal seiches.

propagation in the positive (negative) x direction. By combining the results from the cross-spectral analysis with the upward phase propagation obtained in the FEOF analysis, we see that the observed motions at 80 m with the same frequency as the lowest-frequency internal seiche can be explained by an internal wave radiating downward into the fjord.

How is this wave related to the internal seiches and with the three-layer model? As mentioned in the introduction, a wave on a pycnocline bounding a weakly stratified layer leaks energy to obliquely propagating waves (Kantha 1979; Baines 1982). These change their properties after reflection from a sloping bottom and become unavailable for the pycnocline wave. If the energy flux in these waves is small relative to the energy flux connected with the pycnocline movements, a layered model is a good approximation for the pycnocline movements. But naturally, such a model cannot predict the motions connected with the obliquely propagating waves.

Before estimating the energy flux related with the obliquely propagating wave it is interesting to investigate the origin and end of the ray connected with this wave. Figure 11 shows a long section of the fjord with a net of characteristic curves corresponding to the stratification on day 245 and frequency 0.023 cph. The characteristic curves have tangents with slope $\omega/(N^2 - \omega^2)^{1/2}$, and the energy in internal waves of angular frequency ω follows these curves or rays. It is seen that rays emerging from the sill are crossing M1s between 90 and 60 m, which means that the internal wave at 80 m is probably emanating from the sill region. A very prominent feature in Fig. 11 is that most of the topography in the basin water is parallel to the characteristic curves at the same depth. In other words, most of the bottom topography is critical to the 43-h-period wave with the given stratification. The rays from the sill hit the bottom at a section with close-to-critical slope. On reflection from the bottom, the wave energy is therefore transformed to much smaller scales and is subject to overturning, breaking, instabilities, nonlinear interactions, or other types of destructive phenomena taking the energy out of the wave and supplying it to turbulence (Eriksen 1985).

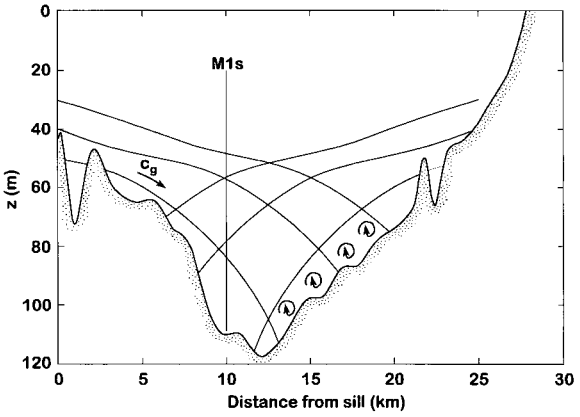

FIG. 11. Long-section of fjord, showing deepest topography and selected characteristics corresponding to stratification at day 245 and frequency 0.023 cph.

The total energy flux, F_b, which radiates into the basin water, in the obliquely propagating wave can be estimated by integrating the horizontal energy flux at M1w over the ray tube emanating from the sill

$$F_b = \int_{z_1}^{z_2} F_x W \, dz, \tag{25}$$

where F_x is the horizontal energy flux, W is the fjord width, and $z_{1(2)}$ are the z coordinate at the bottom and the top of the ray tube at M1w. The horizontal energy flux can be written as

$$F_x = \frac{1}{2}\rho u_0^2 c_{gx}, \tag{26}$$

where u_0 is the horizontal velocity amplitude and c_{gx} is the horizontal group velocity. For a low-frequency wave ($\omega \ll N$) subject to the WKBJ approximation the horizontal group velocity is

$$c_{gx} = \frac{N}{m}, \tag{27}$$

where m is the vertical wavenumber.

In order to estimate the total energy flux we need to determine the vertical extent of the downward ray tube at M1w, the horizontal velocity amplitude, u_0, and the horizontal group velocity, c_{gx}. As mentioned above, the downward rays from the sill region pass the vertical section at M1w between the bottom and depth 60 m, so we set $z_1 = -H$, and $z_2 = -60$ m. The horizontal velocity amplitude is found from spectral analysis as

$$u_0 = \sqrt{2}\left(\frac{\int_{f_1}^{f_2} S(f)\, df}{f_2 - f_1}\right)^{1/2}, \tag{28}$$

where S is the velocity spectrum and $[f_1; f_2]$ is the frequency band. The factor $2^{1/2}$ is the ratio between the amplitude and the rms value. Consistent with the investigations in section 4, we average in the frequency band $f_1 = 0.01$ cph to $f_2 = 0.07$ cph. A representative value for N below 60 m is $N = 0.006$ s^{-1}. The value for m is found from

$$m = \partial\theta/\partial z, \tag{29}$$

where θ is the phase. Using the phase of the first FEOF mode in the frequency band 0.018–0.034 cph presented in section 3 we get an average value of $m = 0.07$ m^{-1} below 60 m. The total energy flux into the basin water can now be calculated from (25)–(27). The result is $F_b = 3.0$ kW. Although this estimate is relatively sensitive, especially to the choice of fre-

quency band and integration levels, it is in the right order of magnitude. The value corresponds to only 2% of the energy put into the internal seiches. This means that the energy flux into the basin water is not very important for the total energy fluxes in the internal seiche. Most of the energy flux connected with the internal seiches is related to the pycnocline movements. This also means that the large-amplitude motions in the basin water are neither important for the period or structure of the internal seiche, nor for the damping of the seiche. Most of the damping must be caused by side friction and shear instabilities in the upper layers. The downward radiating energy may, however, be important for mixing in the basin water. If we, as mentioned above, assume that the downward propagating energy is dissipated in the basin water after near-critical reflection from the bottom, some of this energy is used to mix the basin water and increase the potential energy. In Arneborg and Liljebladh (2001) the energy flux into internal tides is estimated to be 3 kW in the summer period, but the magnitude in the winter period must be about the same. Assuming that all this energy dissipates in the basin water we see that the energy dissipations from internal tides and from internal seiches are of the same order of magnitude. This suggests that the internal seiches are as important for the basin water mixing as are the tides, and this subject is investigated further in Arneborg and Liljebladh (2001).

6. Concluding remarks

We have investigated the internal seiches in Gullmar Fjord based on high-resolution mooring data from a winter period and a summer–fall period in 1997. In both periods the internal seiches manifest themselves with large-amplitude motions in the basin water with period 1–3 days. Above sill level the internal seiches can also be deduced from velocity spectra, but here they are less distinct due to larger energy levels at other frequencies. An interesting property of the basin water motions is that there seems to be upward phase propagation, which is not compatible with a purely standing wave.

In order to show that the observed motions are seiche motions, we have set up an analytical three-layer model, taking into account blocking of the lower layer by the sill. An interesting result of the model is that the vertical modes are coupled by the topography at the mouth, which means that each of the infinite number of basin modes consist of a superposition of both vertical modes. The two spectral peaks in the summer period observations are well predicted as the two lowest-frequency seiches in the three-layer model. The lowest-frequency seiche has the main vertical motions taking place on the upper pycnocline, and the horizontal structure is that of a quarter wave with a node at the sill. The second seiche has the main vertical motions taking place on the lower pycnocline, the horizontal structure being a half wave with a node in the middle of the basin. FEOF analyses of velocity spectra show that the main characteristics of the vertical velocity structures are well predicted by the model.

The forcing and damping of the seiches is estimated from wind data and from mooring data close to the mouth of the fjord. In the winter period the local-wind input into seiche motions is found to be on average 60 kW, while input through coastal pycnocline oscillations via the mouth are found to contribute 81 kW. The latter number may be slightly overestimated because some of the energy is dissipated in the mouth so it does not contribute to the seiches. The damping timescale is estimated from energy budget considerations. The *e*-folding time is found to be approximately equal to the seiche period, which explains the observed quick damping of the seiches when the forcing turns off. That the seiches are observed often and with large amplitudes must be due to near resonance of the forcing. For example, the seiche period, which varies between 1 and 3 days depending on the stratification, is close to the timescale for the low pressure systems coming in from the west.

Ice cover at the inner parts of the fjord during part of the winter period may have influenced the relation between local wind forcing and coastal forcing. One effect of an ice cover is that our wind-input estimate is too large. Furthermore, the winter period may not be representative for the whole year, so our estimate of the forcing by local wind relative to coastal forcing may differ from the annual mean.

The large amplitude oscillations in the basin water with upward phase propagation are explained as downward-radiating internal waves, emanating at the sill, and dissipating after near-critical reflection from the sloping fjord bottom. The energy flux in these waves is only 2% of the energy put into the internal seiches, which means that they are not important for the period, structure, or damping of the internal seiches. The main energy flux connected with the internal seiches is related to pycnocline movements, and this explains why the three-layer model gives reasonable results. This also means that the seiches are mainly damped by shear instabilities and side friction in the upper layers. The downward radiating wave is, however, important for the basin water mixing, as is treated in more detail in Arneborg and Liljebladh (2001).

It is clear that the downward propagating waves are an inherent property of the internal seiches. The internal seiches exist on a real stratification that is a mix between a continuous stratification and a layered structure, which means that energy leaks out from the pycnocline movements. We have, however, not been able to propose the actual relation between the internal seiche energy and the energy flux lost to the basin water. One way to investigate further into this is to use a linear-theory two-dimensional model similar to the one presented in Tverberg et al. (1991), which takes into account real strat-

ification and topography. It is, though, essential that the energy loss related with near-critical reflection is properly described, which is no trivial task.

Acknowledgments. During this work L. Arneborg was supported by a grant from the Danish Research Council, while B. Liljebladh and the field measurements were supported by a grant to Anders Stigebrandt from the Swedish Natural Science Research Council (NFR). The meteorological data and some CTD profiles were obtained from Kristineberg Marine Research Centre. We wish to thank the crews on R/V *Skagerak* and R/V *Arne Tisselius*, and Stefan Hamilton and Karin Gustafsson for help with the field work, Oscar Pizarro for help with the FEOF analyses, Agneta Malm for help with figures, and Anders Stigebrandt for helpful comments on the manuscript.

APPENDIX

Boundary Condition at the Fjord Mouth

The instantaneous energy flux out through the fjord mouth can be found as an integral over the fjord mouth of the horizontal velocity multiplied with the pressure (Gill 1982), which can be written as

$$F(t) = -W(p_1(0, t)u_1(0, t)h_1 + p_2(0, t)u_2(0, t)h_2). \quad \text{(A1)}$$

The pressures are related to the upper interface elevation through

$$p_2 - p_1 = \rho g_1' \eta_1. \quad \text{(A2)}$$

Under the rigid-lid assumption, the baroclinic velocities in the fjord mouth must fulfill the condition

$$u_1(0, t)h_1 + u_2(0, t)h_2 = 0. \quad \text{(A3)}$$

Per definition the baroclinic pressures in the fjord mouth must also fulfill

$$p_1(0, t)h_1 + p_2(0, t)h_2 = 0. \quad \text{(A4)}$$

Combining (A1)–(A4) it is possible to write the instantaneous energy flux out through the mouth as

$$F(t) = \rho g_1' \eta_1(0, t)Q_1(0, t) = -\rho g_1'(0, t)Q_2(0, t), \quad \text{(A5)}$$

where $Q_{1(2)}$ are the volume fluxes in the upper (lower) layers,

$$Q_i = Wh_i u_i, \qquad i = 1, 2. \quad \text{(A6)}$$

Since the baroclinic energy flux, F, and the baroclinic volume fluxes, Q_i, are both assumed continuous at the mouth, the relation $Z = F/Q^2$ must also be continuous. The advantages of Z, which is an impedance [see Gill (1982) for the case of a surface seiche], is that it is independent of the seiche amplitude. From (A5) and (A6) we obtain

$$Z(t) = \frac{\rho g_1' \eta_1(0, t)}{Wh_1 u_1(0, t)}. \quad \text{(A7)}$$

The upper-layer velocity can be found from (5) and (9):

$$u_1(0, t) = -\frac{j}{h_1} \sum_{n=1}^{2} A_n c_n \sin\left(\frac{\omega L}{c_n}\right) e^{-j\omega t}. \quad \text{(A8)}$$

Using (9), (10), and (A8), (A7) can be written as

$$Z(t) = -\frac{j\rho g_1'}{W} \frac{\mu_2 \mu_1}{\mu_2 - \mu_1} \left(\frac{1}{\mu_1 c_1} \cot\left(\frac{\omega L}{c_1}\right) - \frac{1}{\mu_2 c_2} \cot\left(\frac{\omega L}{c_2}\right)\right). \quad \text{(A9)}$$

In the coastal two-layer stratification the internal coastal Kelvin wave can be written as

$$\eta = \eta_0 e^{x/a} e^{j(ky - \omega t)}, \quad \text{(A10)}$$

where the internal Rossby radius a_i is given by

$$a_i = \frac{c_i}{f} = \frac{1}{f}\left(\frac{g_1' h_1 h_2}{h_1 + h_2}\right)^{1/2} \quad \text{(A11)}$$

and $k = \omega/c_i$ is the wavenumber. It can be shown that the ratio of the energy flux to the square of the baroclinic volume transport in the internal Kelvin wave can be written as

$$Z(t) = \frac{1}{2} \frac{\rho g_1'}{c_i a_i}. \quad \text{(A12)}$$

Combining (A9) and (A12) we obtain

$$\frac{1}{2} \frac{W}{a_i} = -j \frac{\mu_2 \mu_1}{\mu_2 - \mu_1} \left(\frac{c_i}{\mu_1 c_1} \cot\left(\frac{\omega L}{c_1}\right) - \frac{c_i}{\mu_2 c_2} \cot\left(\frac{\omega L}{c_2}\right)\right). \quad \text{(A13)}$$

REFERENCES

Arneborg, L., and B. Liljebladh, 2001: The internal seiches in Gullmar Fjord. Part II: Contribution to basin water mixing. *J. Phys. Oceanogr.*, **31,** 2567–2574.

Baines, P. G., 1982: On internal tide generation models. *Deep-Sea Res.*, **29,** 307–338.

Djurfeldt, L., 1987: On the response of the fjord Gullmaren under ice cover. *J. Geophys. Res.*, **92,** 5157–5167.

Eriksen, C. C., 1985: Implications of ocean bottom reflection for internal wave spectra and mixing. *J. Phys. Oceanogr.*, **15,** 1145–1156.

Farmer, D. M., 1978: Observations of long nonlinear internal waves in a lake. *J. Phys. Oceanogr.*, **8,** 63–73.

Gill, A. E., 1982: *Atmosphere–Ocean Dynamics.* Academic Press, 662 pp.

Kantha, L. H., 1979: On leaky modes on a buoyancy interface. *Dyn. Atmos. Oceans*, **3,** 47–54.

Lemmin, U., and C. H. Mortimer, 1986: Tests of an extension to internal seiches of Defant's procedure for determination of surface seiche characteristics in real lakes. *Limnol. Oceanogr.*, **31,** 1207–1231.

Maas, L. R., and F.-P. A. Lam, 1995: Geometric focusing of internal waves. *J. Fluid Mech.*, **300,** 1–41.

Monismith, S. G., 1985: Wind-forced motions in stratified lakes and their effect on mixed-layer shear. *Limnol. Oceanogr.*, **30,** 771–783.

Münnich, M., A. Wüest, and D. M. Imboden, 1992: Observations of

the second vertical mode of the internal seiche in an alpine lake. *Limnol. Oceanogr.*, **37,** 1705–1719.
Parsmar, R., and A. Stigebrandt, 1997: Observed damping of barotropic seiches through baroclinic wave drag in the Gullmar Fjord. *J. Phys. Oceanogr.*, **27,** 849–857.
Shaffer, G., and L. Djurfeldt, 1983: On the low-frequency fluctuations in the eastern Skagerrak and in Gullmaren. *J. Phys. Oceanogr.*, **13,** 1321–1340.
Spiegel, R. H., and J. Imberger, 1980: The classification of mixed-layer dynamics in lakes of small to medium size. *J. Phys. Oceanogr.*, **10,** 1104–1121.
Thorpe, S. A., 1974: Near-resonant forcing in a shallow two-layer fluid: A model for the internal surge in Loch Ness? *J. Fluid Mech.*, **63,** 509–527.
Tverberg, V., B. Cushman-Roisin, and H. Svendsen, 1991: Modeling of internal tides in fjords. *J. Mar. Res.*, **49,** 635–658.
Wiegand, R. C., and V. Chamberlain, 1987: Internal waves of the second vertical mode in a stratified lake. *Limnol. Oceanogr.*, **32,** 29–42.
Zeilon, N., 1913: On the seiches of the Gullmar Fjord. *Sven. Hydrgr.–Biol. Komm. Skr.*, **V,** 1–17.